

A multilayer biochemical dry deposition model

2. Model evaluation

Yihua Wu¹

National Exposure Research Laboratory, Environmental Protection Agency, Research Triangle Park, North Carolina, USA

Bart Brashers,² Peter L. Finkelstein,³ and Jonathan E. Pleim³

Atmospheric Science Modeling Division, Air Resources Laboratory, NOAA, Research Triangle Park, North Carolina, USA

Received 13 March 2002; revised 12 July 2002; accepted 22 July 2002; published 9 January 2003.

[1] The multilayer biochemical dry deposition model (MLBC) described in the accompanying paper was tested against half-hourly eddy correlation data from six field sites under a wide range of climate conditions with various plant types. Modeled CO₂, O₃, SO₂, and H₂O (latent heat) fluxes were compared with measurements. Model outputs have good correlations with measurements at all locations. Correlation coefficients between model outputs and measurements at all sites range from 0.72 to 0.96 for CO₂ flux, from 0.84 to 0.98 for H₂O flux, from 0.77 to 0.95 for O₃ flux, and from 0.36 to 0.86 for SO₂ flux. Model sensitivity analyses were conducted to investigate the variation of model outputs due to measurement errors of input variables and to changes of environmental conditions such as changes in weather conditions. The MLBC outputs were also compared with outputs from the Multilayer Model (MLM) model [Meyers *et al.*, 1998] and the Regional Acid Deposition Model (RADM) [Wesely, 1989] at two typical sites.

Comparisons show that the MLBC performs better than the other two models. The model is suitable for use in nationwide dry deposition networks, for example, the Clean Air Status And Trends Network (CASTNet). It can be used to assist in describing total pollutant loadings to major ecosystems. With some modifications, the model may also be suitable for inclusion in region (meso-) scale numerical models, for example, the Community Multiscale Air Quality (CMAQ) model.

INDEX TERMS: 0315 Atmospheric Composition and Structure: Biosphere/atmosphere interactions; 0322 Atmospheric Composition and Structure: Constituent sources and sinks; 3307 Meteorology and Atmospheric Dynamics: Boundary layer processes; 3322 Meteorology and Atmospheric Dynamics: Land/atmosphere interactions; 1615 Global Change: Biogeochemical processes (4805); *KEYWORDS:* multiplayer, biochemical, dry, deposition, model

Citation: Wu, Y., B. Brashers, P. L. Finkelstein, and J. E. Pleim, A multilayer biochemical dry deposition model, 2, Model evaluation, *J. Geophys. Res.*, 108(D1), 4014, doi:10.1029/2002JD002306, 2003.

1. Introduction

[2] In the accompanying paper, we described a multilayer biochemical (MLBC) dry deposition model. The MLBC is a resistance model, an analog to Ohm's law. However, some detailed biochemical processes that affect dry deposition are considered in the model. Parameterizations of aerodynamic, boundary layer, stomatal, cuticular and soil surface resistances are updated with new findings in recent research. The model is designed for use in nationwide dry deposition networks, e.g. the Clean Air Status And Trends Network (CASTNet); and in mesoscale air quality models, e.g. the

Community Multiscale Air Quality model (CMAQ). In order to investigate the application potential of the model to CASTNet data as well as in determining total pollutant loadings to major ecosystems, results of model performance evaluation and model sensitivity tests are described in this paper. To evaluate the model, representative samples of eddy covariance (EC) flux measurements were selected from six field programs: three agricultural sites, two forest sites and one pasture site. The temporal resolution of the data sets at the six sites are half hourly. However, data were selectively used in this study based on the data quality control of Meyers *et al.* [1998]. Parallel runs of the Multilayer Model (MLM) [Meyers *et al.*, 1998] and Regional Acid Deposition Model (RADM) [Wesely, 1989] were conducted for model comparisons. Results from these parallel runs were compared using Taylor's [2001] diagrams, which provides a concise statistical summary of how well models match observations in terms of their correlation, their centered pattern root-mean-square difference, and the difference in their variances. Numerical tests

¹Now at Hydrological Sciences Branch, NASA Goddard Space Flight Center, Greenbelt, Maryland, USA.

²Now at MFG Inc, Lynnwood, Washington, USA.

³On assignment at Atmospheric Modeling Division, U.S. Environmental Protection Agency, Research Triangle Park, North Carolina, USA.

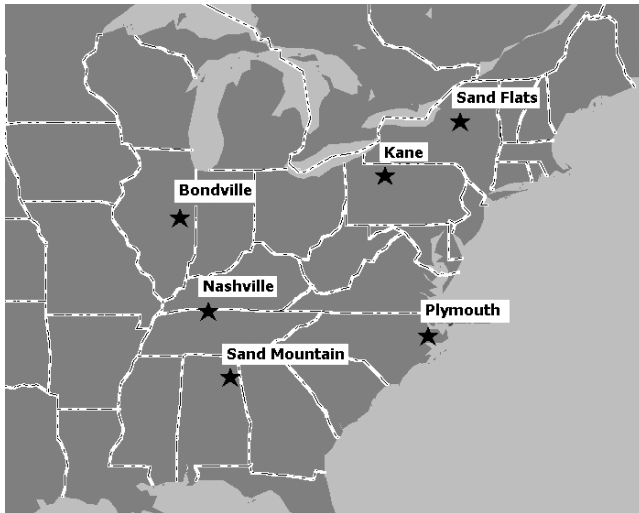


Figure 1. Locations of the six field sites.

were also conducted to investigate model sensitivity to weather condition variations and measurement errors of input variables. Site and data descriptions are given in section 2, and the model evaluation is presented in section 3. A short summary is presented in section 4.

2. Site Description

[3] Data collected from six field programs were used in this study. These field programs include studies over a pasture in Sand Mountain, Alabama, a soybean field near Nashville, Tennessee, a soybean field near Plymouth, North Carolina, a corn field near Bondville, Illinois, a deciduous forest near Kane Forest, Pennsylvania, and a mixed (deciduous and coniferous) forest in the Sand Flats State Forest in the Adirondack region of New York. The locations of the sites are shown in Figure 1. Each of these sites had uniform fetches of at least 1/2 km (crop field) to usually more than 1 km (forest areas) in the sampling sector. Briefly environmental conditions at each site are described in the corresponding subsection below. More details on the Sand Mountain, Bondville and Nashville sites are given by Meyers *et al.* [1998]. Details on Kane Forest and Sand Flats are given by Finkelstein *et al.* [2000]. The data collection period and plant type for each site is summarized in Table 1.

[4] The measurement techniques at all sites were the same. Two major instrument systems were used in these experiments: the fast response and the slow response instruments. Monitoring equipment used in the experiment included a three-axis sonic anemometer and fast response gas analyzers. Measurements were taken at 10 Hz, and

collected over half-hour periods. Fluxes of momentum, heat (sensible and latent), ozone, sulfur dioxide, and carbon dioxide were computed. Other measurements, including net-radiation and soil-heat flux were available, and used as a data quality check. Data for each half-hour period were considered valid if all the following conditions were met; the total energy balanced within ± 100 watts/m², the average wind direction brought the flow from an unobstructed sector, there were no significant trends in any variable, the vertical rotation angle needed to require the average vertical velocity, w , to be equal to zero was less than or equal to two degrees, and the instrument calibrations were within normal operating parameters. Instruments at the various sites were mounted approximately 5 m above the top of the crop, or, in the case of the forest sites, on a 36 m guyed, walk-up, scaffold tower. Chemical analyzers were housed in an air-conditioned box near the base of the tower, or in shelters built on the tower at the forest sites. Wind velocity and turbulence were measured with an ATI sonic anemometer. O₃ and SO₂ were sampled from a draft tube with the inlet immediately adjacent to the sonic. Fast response measurements of O₃ were made with a specially constructed analyzer that uses the chemiluminescent reaction of O₃ with eosin-y dye. Fast response SO₂ measurements were taken with a modified Meloy SA285-E total sulfur analyzer. Soil temperature and soil heat flux were measured near the base of the tower. Leaf area index (LAI) and stomatal resistance measurements were made at several locations throughout the canopy. At the agricultural sites, the heights for temperature gradient measurements were about 1 to 2 m for the lower point and 8 to 10 m for the higher point. At the forest sites, the temperature gradient was measured between 24 and 36 m. Leaf area index (LAI) was measured weekly using a Licor 2000T plant canopy analyzer. The reader is referred to Meyers *et al.* [1998] for a more detailed description about the system design, the flux instrumentation, data collection, and data quality procedures.

2.1. Sand Mountain, Alabama

[5] The Sand Mountain site was located about 1 km south of Crossville, AL. The measurement site was on a slight knoll at an elevation of 347 m with a downward slope of about 1% in all directions. The vegetation surrounding the site consisted of unevenly distributed pasture of fescue (52%), blue grass (20%), and white clover (20%). Conditions were relatively wet from the latter part of April into early May. Precipitation was then generally very light through early June, when significant rain was measured at the site. Surface moisture was generally adequate for good growth throughout the period. Leaf area index (LAI) increased from about 1.0 on April 15 to about 2.3 by June 13. The height of the clumped grass increased from 10 to 30

Table 1. Site Summary

Site	Location	Latitude/Longitude	Plants	Operation Period
SAND	Sand Mtn, AL	34.29N/85.97W	Pasture grass (C ₄)	04/14/95–06/13/95
NASH	Nashville, TN	36.65N/87.03W	Soybean (C ₃)	06/22/95–10/11/95
PLYM	Plymouth, NC	35.70N/76.80W	Soybean (C ₃)	07/17/96–08/15/96
BOND	Bondville, IL	36.65N/87.03W	Corn (C ₄)	08/18/94–10/01/94
KANE	Kane Forest, IL	41.60N/78.80W	Deciduous forest (C ₃)	04/29/97–10/24/97
SFTS	Sand Flats, NY	43.60N/75.20W	Mixed forest (C ₃)	05/12/98–10/19/98

cm over the same period, in spite of cows grazing in the field.

2.2. Nashville, Tennessee

[6] The Nashville site was set up in a soybean field, about 60 km NNW of Nashville. Elevation of the site is 585 m with a gentle NW–SE slope of about 1.5%. The gently-rolling uniform fetch over the soybean crop extended to at least 1500 m through the SE and southern quadrants. A cornfield was adjacent to the soybeans, 140 m to the west at the closest point. The instrument boom was 4.55 m AGL and oriented to 208E. The lower point was incrementally increased to 2 m as the crop grew.

[7] The soybeans were planted on June 13, and went through a rapid growth period from July 10 through August 5 with the LAI increasing from 1 to about 6. Midday plant leaf resistance was about 80 sec/m (measurements from a Licor LI-1600T porometer), and the crop reached a maximum height of 1.2 m. Precipitation was light after late July and by mid August the beans were drought stressed. Leaf resistance increased to about 800 sec/m and the LAI gradually decreased to about 3 by the end of September. By October 11 the LAI decreased to about 1 when the beans were mostly stalks and pods.

2.3. Plymouth, North Carolina

[8] The Plymouth site was set up in a soybean field on a farm about 10 miles south of Plymouth, NC. The area was very flat, with no obstructions to the flow for over 1 km in the sampling acceptance sector. As part of a multilaboratory field program to look at NO_x emissions from soils, the term of this experiment was short, starting July 15 and concluding August 15, 1996. At the start of the experiment, the crop was approximately 0.5 m high, with an LAI of 3. By the end of the experiment, the crop was 1 m high, and the LAI was 6. The field was regularly irrigated and soil moisture was adequate for good plant growth throughout the experiment.

2.4. Bondville, Illinois

[9] The Bondville study took place at the University of Illinois Soil and Crop Experimental Station located 6.9 km south of Bondville, IL. The general terrain surrounding the site was flat, open farmland. The measurement site was situated at the north edge of a cornfield to measure fluxes with winds from the southerly direction. Data collection was initiated August 18, 1994 and continued until October 1. At the start of the experiment the corn was 1.8 to 2.4 m high including tassels, and actively growing. By September 2, the corn was maturing and the bottom leaves were turning brown. By September 21, 60% of the corn leaves were brown, and by October 3 essentially all the leaves were brown. LAI was 3.0 on August 18, increased to 3.3 by the end of August and then slowly decreased to 2.5 by October 1. The LAI remained at about 2.5 until October 14 when the corn was harvested.

2.5. Kane Experimental Forest, Pennsylvania

[10] The Kane Experimental Forest is located adjacent to the Allegheny National Forest in northwestern Pennsylvania. The area is on the top of a plateau, with gently rolling topography and changes in elevation of 15 to 30 meters within 1500 meters of the site. There was a slight rise due east of the site. South of the site the terrain sloped down

gradually to Wolf Run, a creek, then rose to a ridge at about the same elevation as the site approximately 2 km away. The tree canopy was nearly uniform in height. There were no major point sources or roads within 30 km of the site.

[11] In the vicinity of the experiment, there was a mix of tree species, 38% Black Cherry (*Prunus serotina*), 34% Red Maple (*Acer rubrum*), 23% Sugar Maple (*Acer saccharum*), and 5% others, of which a fair part are Eastern Hemlock (*Tsuga canadensis*), that tend to grow adjacent to the stream beds. The canopy was 22 to 23 meters high. The forest in this area is second growth, but has not been logged in more than 50 years. The area is in a slight depression, and because there are plentiful springs at higher elevation, the soil was moist throughout the year. Because of a late spring, leaf bud did not occur until approximately the second week of May. Leaves were senescent on all the major deciduous species by the middle of October.

2.6. Sand Flats, New York

[12] The observation site was in the Sand Flats State Forest, in Lewis County, New York; about 7 miles NE of Boonville, NY, and on the southwest boundary of the Adirondack Park. The Sand Flats site was in a mixed coniferous - deciduous forest. Observations were taken from May 12, 1998 to October 20, 1998. The tower was 36 m tall. The forest is second growth, most naturally seeded, but there are some areas of planted pines from the Civilian Conservation Corps era of the late 1930's. Some thinning has occurred, as directed by the New York State Forest Service. Composition of the forest in the sector to the west of the tower, toward which the anemometer was pointing, includes 20% Eastern White Pine (*Pinus strobus*), 20% Black Cherry (*Prunus serotina*), 17% Sugar Maple (*Acer saccharum*), 15% Eastern Hemlock (*Tsuga canadensis*), 10% White Spruce (*Picea glauca*), 8% open space, and a scattering of Red Maple (*Acer rubrum*), Elm (*Ulmus sp.*), Balsam Fir (*Abies balsamea*) and Yellow Birch (*Betula lutea syn. alleghaniensis*). Because of the mix of species, the vertical structure of the forest was quite different from that at Kane, with a much higher density of branches and needles at lower levels on the conifers mixing with the higher leaves of the deciduous trees. The topography of the area is quite flat within 0.5 km of the tower, and somewhat irregular beyond that distance. The nearest roads were 300 m east of the tower, and 800 m north. Traffic on both was light.

3. Model Evaluation

[13] To evaluate the MLBC model, model performance analysis and sensitivity tests were conducted, and presented respectively in the following subsections. Values of some key input constants are given in Table 2. Downward fluxes are defined as negative while upward fluxes are defined as positive in this study.

3.1. Model Performance

[14] Three analyses were conducted to investigate the MLBC performance: comparisons of modeled and measured fluxes of CO₂, O₃, SO₂ and latent heat (H₂O), analysis of modeled seasonal and diurnal cycles, and comparison with other models. The single-diagram method

Table 2. Values of Input Variables Used in the Model ($Q_t = [T_c - 25]/10$)^a

Parameter	Unit	Values by Plant Type				
		Pasture Grass (C ₄)	Soybean (C ₃)	Corn (C ₄)	Deciduous Forest (C ₃)	Mixed Forest (C ₃)
Maximum rubisco capacity (V_m)	$\mu\text{mol m}^{-2} \text{s}^{-1}$	50.0	100.0	100.0	85.0	85.0
Minimum stomatal conductance (b)	$\mu\text{mol m}^{-2} \text{s}^{-1}$	4000.0	1500.0	4000.0	2500.0	2500.0
Stomatal conductance slope factor (m)	dimensionless	9.0	9.0	9.0	9.0	9.0
Rubisco inhibition constant for O ₂ (K_o)	pa	$3 \times 10^4 \times 1.2^{Q_t}$	$3 \times 10^4 \times 1.2^{Q_t}$			
Rubisco Michaelis-Menten constant for CO ₂ (K_c)	pa	30.0×2.1^{Q_t}	30.0×2.1^{Q_t}	30.0×2.1^{Q_t}	30.0×2.1^{Q_t}	30.0×2.1^{Q_t}
Hyperbolic photosynthesis coupling coefficient (α)		0.95	0.95	0.95	0.95	0.95
Hyperbolic photosynthesis coupling coefficient (β)		0.85	0.85	0.85	0.85	0.85

^a Values specified according to *Sellers et al.* [1996], *Wang and Leuning* [1998], *Wilson et al.* [2000a] and J.A. Berry (personal communication, 1999).

described by *Taylor* [2001] was used for comparisons. This method provides a concise statistical summary of how well model outputs match measurements in terms of their correlation, their standard deviations, and centered pattern root-mean-square difference. The correlation coefficient (R) is shown as the radial angle, the standard deviations (σ_m for model and σ_o for observations) as the radial distance. The observations are plotted on the horizontal axis since they are perfectly correlated with themselves ($R = 1$). The centered pattern root-mean-square difference (E') is the vector distance between the observation (on the horizontal axis) and the corresponding modeled point. The relationship between E' and R , σ_m and σ_o can be expressed as $E' = \sqrt{\sigma_o^2 + \sigma_m^2 - 2\sigma_o\sigma_m R}$. The larger the correlation coefficient, the better the match between the modeled and observed phases of seasonal and diurnal cycles; the closer the standard deviation of the model to the observation, the better the estimation of the amplitude of variations (seasonal and diurnal cycles); the smaller the centered pattern root-mean-square difference, the closer correspondence between the model and the observations.

3.1.1. Comparisons With Measurements

[15] Both measured and modeled fluxes are half hourly. However, data used in this study are selected based on the data quality control by *Meyers et al.* [1998].

3.1.1.1. CO₂ Fluxes

[16] Figure 2a shows the values of σ_m , σ_o , R and E' for fluxes of CO₂ at the six sites. The correlation coefficients range from 0.72 (Bondville) to 0.96 (Plymouth). These indicate that the model-simulated seasonal and diurnal cycles of CO₂ are better in-phase at Plymouth, NC than at the other sites. The σ_o values range from 0.260 ppm m s⁻¹ (Sand Mountain) to 0.370 ppm m s⁻¹ (Sand Flats) while σ_m values vary from 0.250 ppm m s⁻¹ (Kane Forest) to 0.416 ppm m s⁻¹ (Plymouth). Comparisons of standard deviations between model-simulated and observed data show that the model overestimated the amplitudes of CO₂ variations at Plymouth, Sand Mountain, Nashville, but underestimated at the other three sites. However, the degrees of overestimation and underestimation are not large. The E' value is the largest (0.2557 ppm m s⁻¹) at Bondville and smallest (0.1208 ppm m s⁻¹) at Plymouth, suggesting that the modeled CO₂ flux has closer correspondence to the observations at Plymouth. The figure shows that the contribution of R to E' is larger

than the contribution of standard deviations at most of the sites.

3.1.1.2. H₂O Fluxes

[17] As shown in Figure 2b, the results for latent heat fluxes are very similar to the results for CO₂ fluxes. The lowest R value is at Bondville (0.84) and the highest is at Plymouth (0.97), indicating that the timing of the model-simulated seasonal and diurnal cycles of latent heat fluxes is in better agreement at Plymouth than at the other sites, especially better than at Bondville. Both σ_o and σ_m have their largest value (144.00 and 150.00 W m⁻², respectively) at Plymouth, and smallest (89.00 and 94.00 W m⁻², respectively) at Bondville. As suggested by the comparisons of σ values between model estimations and measurements, the model slightly overestimated the amplitudes of seasonal and diurnal cycles at Plymouth and Sand Flats, but underestimated by a small amount at the other four sites. The E' value is largest (55.37 W m⁻²) at Sand Flats, and smallest (30.00 W m⁻²) at Plymouth. Again, the R has more contribution to E' than the standard deviation at most of the sites.

3.1.1.3. O₃ Fluxes

[18] Shown in Figure 2c, Plymouth again has the highest correlation coefficient (0.95) while Bondville has the lowest one (0.75). The other sites have correlation coefficients in the 0.8 to 0.9 range. The R -values indicate that model-simulated seasonal and diurnal cycles of O₃ flux were in better agreement at Plymouth than at the other five sites. The σ_o ranges from 0.107 ppb m s⁻¹ (Sand Mountain) to 0.199 ppb m s⁻¹ (Kane Forest) while σ_m varies from 0.140 ppb m s⁻¹ (Sand Mountain) to 0.201 ppb m s⁻¹ (Kane Forest). It can be seen from standard deviation values that the model underestimated the amplitude at Plymouth, and overestimated it at Sand Mountain and Nashville. Sand Flats has the largest E' value (0.1364 ppb m s⁻¹) while Plymouth has the smallest one (0.0608 ppb m s⁻¹). The correlation coefficient is the dominant contributor to E' at all sites.

3.1.1.4. SO₂ Fluxes

[19] The correlation coefficients for SO₂ flux range from 0.38 (Sand Flats) to 0.86 (Nashville), as shown in Figure 2d. It is worth pointing out that the correlation for SO₂ flux is the lowest, indicating that it is the most difficult of the fluxes to predict and measure. It should also be noted that

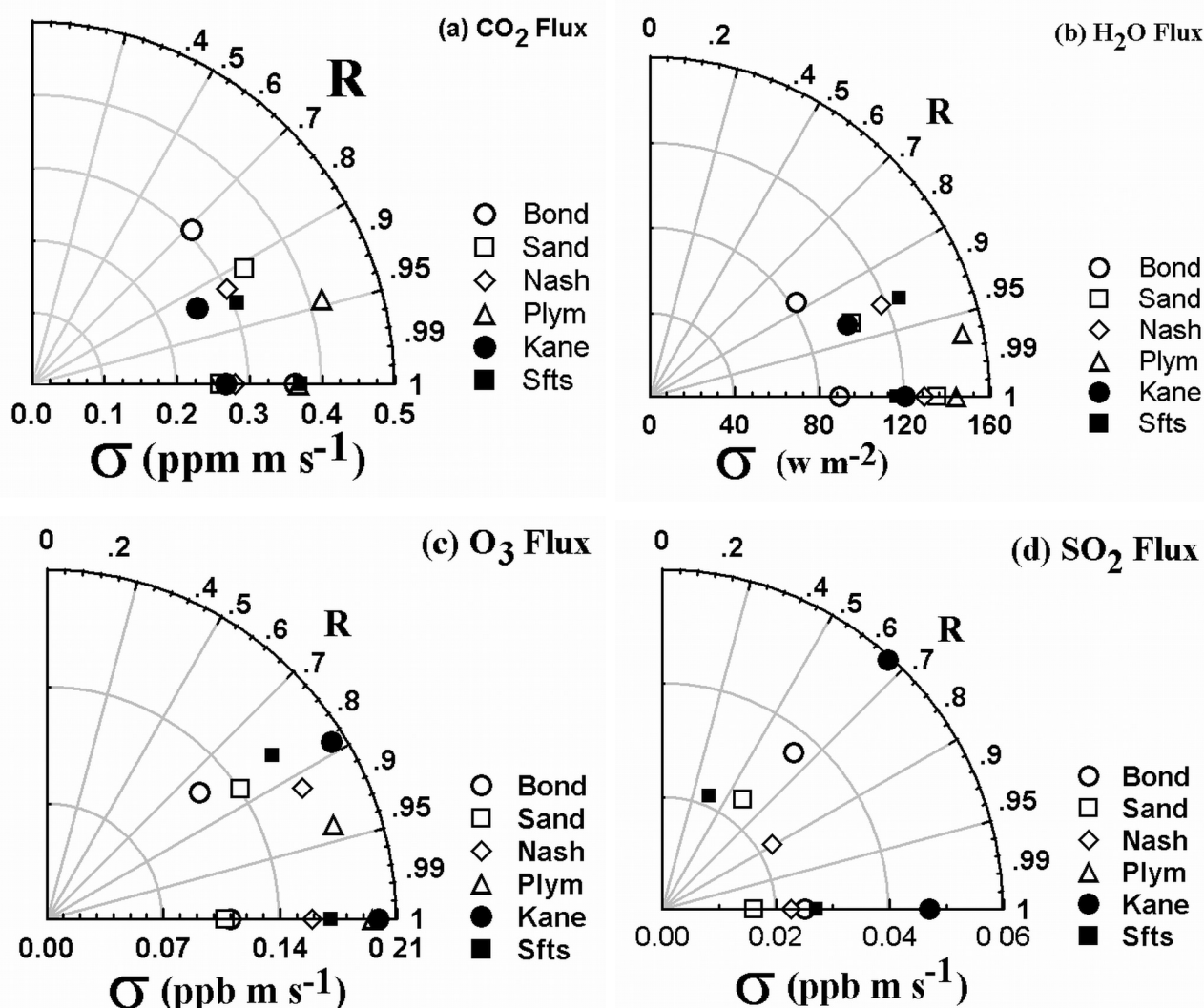


Figure 2. Comparisons between modeled and observed fluxes at the six sites. The time period for each site is given in Table 1. The correlation coefficient (R) is shown as the radial angle, the standard deviations (σ) as the radial distance, and the centered pattern root-mean-square difference (E') as the vector distance between the observation (on the horizontal axis) and the corresponding modeled point, for (a) CO₂ flux, (b) H₂O flux, (c) O₃ flux, and (d) SO₂ flux.

there are fewer observations of SO₂ fluxes at most sites, and especially at Plymouth where SO₂ observations were too few for a valid analysis. The σ_o values are biggest at Kane Forest (0.047 ppb m s⁻¹) and smallest at Sand Mountain (0.016 ppb m s⁻¹). The σ_m values are biggest at Kane Forest (0.059 ppb m s⁻¹) and smallest at Nashville (0.022 ppb m s⁻¹). Shown by the standard deviations, the model overestimated amplitude of seasonal and diurnal cycles at Kane Forest, Bondville, and Sand Mountain. Kane Forest has the largest E' value (0.0342 ppb m s⁻¹) due to both poor correlation and overestimation of the standard deviation. Nashville has the smallest E' (0.00625 ppb m s⁻¹).

[20] To further show the agreement between modeled and measured fluxes, scatterplots of modeled versus measured O₃ and SO₂ fluxes at Nashville, TN are given in Figures 3a–3b. It is clear that there are some scatters for both O₃ and SO₂ fluxes, some low measurements are overestimated,

and some high measurements are underestimated. Scatter is even more significant for SO₂ flux. However, the bias between the model and measurements is low, on average.

3.1.1.5. Discussion

[21] Plants at Bondville and Sand Mountain are C₄ plant type while plants at the other four sites are C₃ plants. The correlation coefficients for CO₂, H₂O and O₃ are relatively higher for C₃ plants than those for C₄ plants, suggesting that the photosynthesis model works better for C₃ plants than for C₄ plants. The scheme for C₄ plant photosynthesis proposed by *von Caemmerer and Furbank* [1999] considers more variables, and may be worth testing in future studies. Overall, the model performance is relatively better at Plymouth and Nashville than at the other four sites. There are several possible reasons. The first one is probably that the plant canopy at Plymouth and Nashville (Soybean) is more homogeneous than the plant canopy at mixed forest sites

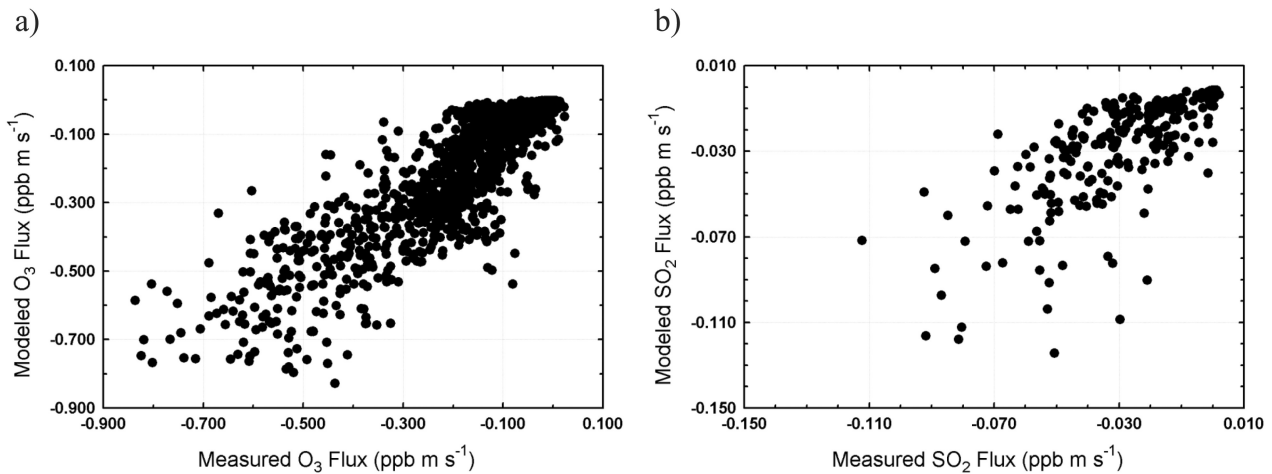


Figure 3. Scatterplots of modeled versus measured fluxes for O₃ and SO₂ at Nashville, TN from June 22 through October 11, 1995. (a) O₃ flux (ppb m s⁻¹), (b) SO₂ flux (ppb m s⁻¹).

with an inhomogeneous canopy where measurements are harder to interpret and model scaling is more difficult. The second one is that the photosynthesis process for C₃ metabolism is better parameterized.

3.1.2. Seasonal and Diurnal Cycles

[22] We selected two sites for this analysis, Kane Forest and Nashville, where data were gathered throughout the full growing season. The weekly daytime (Local time 09:00–15:00) averages and average hourly values of modeled CO₂, O₃, SO₂ and H₂O fluxes, and the corresponding measurements at these two sites, are used to illustrate the modeled seasonal and diurnal cycles. They are representative of the other sites.

3.1.2.1. Kane Forest Site

[23] Figure 4 shows the weekly average daytime fluxes of CO₂, O₃, SO₂ and H₂O. Generally, all fluxes increase in spring, reach a plateau in summer, decrease in fall, and drop to a minimum in winter. The modeled seasonal cycles match the observed data quite well. Modeled amplitudes are larger than observed for CO₂, O₃, and SO₂ fluxes, but smaller than observed for latent heat flux. The figure also indicates that the model overestimated CO₂, O₃, SO₂ fluxes, but underestimated H₂O flux for the whole season.

[24] The diurnal cycles of observed and modeled CO₂, O₃, SO₂ and H₂O fluxes are shown in Figure 5. All fluxes start to increase after local time 05:00, reach their maximum around noontime, then decrease significantly, and reach their minimum after local time 20:00. Similar to the seasonal cycles, modeled phases have good agreement with observations, but modeled amplitudes are larger than observed for CO₂, O₃, SO₂ fluxes, and smaller than observed for H₂O fluxes. There were some cases in which the observed latent heat fluxes were very close to the observed global solar radiation. The model missed these high values, resulting in underestimation in both the weekly daytime averages and hourly averages. There are three possible reasons. First, the model does not compute an energy balance for layers within the canopy, but latent heat flux is usually tied to, and constrained by, the energy balance. Second, leaf temperature used in the model is neither computed from the energy balance, nor a leaf

temperature measurement. It is estimated by extrapolating the surface (log-) layer profile to the displacement height, subject to some constraints. It could be lower than the actual leaf temperature, which will lead to underestimation of latent heat fluxes and bias in modeled CO₂, O₃ and SO₂ fluxes. Third, the model does not include evaporation of surface water from wet leaves in the model. After a rainfall and when the sun comes out, evaporation from wet leaves is quite significant.

3.1.2.2. Nashville Site

[25] The weekly daytime averages of CO₂, O₃, SO₂, and H₂O fluxes at Nashville are given in Figure 6. Most of the time, model simulations are in good agreement with observations. The model-simulated amplitudes are about the same as the observed. The model overestimated the CO₂ flux early in the season, but missed the secondary peak at week 38 (this could be due to overestimating water stress during the raining period). The model also missed the peak of O₃ flux at week 33. Figure 7 shows that the simulated diurnal cycles of all fluxes at Nashville are in good agreement with the observations. The model slightly overestimated the peak H₂O flux, and shows a systematic error in the net CO₂ flux (which could be due to ignoring soil respiration in the model). The model slightly underestimated O₃ and SO₂ fluxes.

3.1.2.3. Discussion

[26] From the point of view of seasonal and diurnal cycles, it can be seen that the model performance at the Nashville is much better than at Kane Forest. The major reason is likely that the plants at Nashville are soybeans with a very homogeneous canopy while the plants at Kane Forest are a mixed, deciduous forest with an inhomogeneous canopy. Modeled diurnal cycles match with observations better than seasonal cycles. The major reason is that the maximum photosynthetic capacity (V_m) specified in the model did not change with time or plant growth and development stages. Obviously, V_m at plant initial growth stage, rapid growth stage and senescence stage could be very different. *Wilson et al.* [2000a, 2000b] reported that there was extensive variability in V_m as a result of vertical canopy position, species type and leaf age. Dynamic spec-

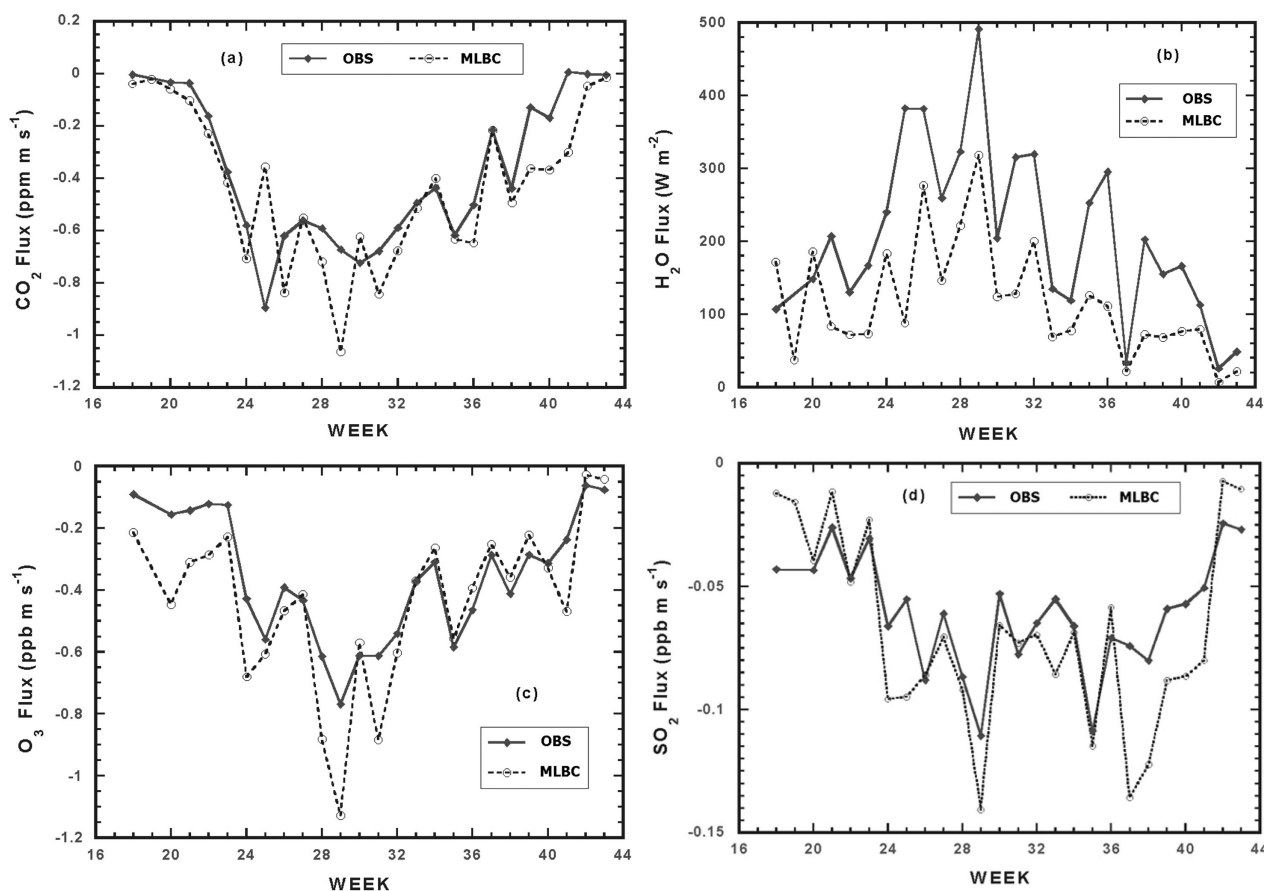


Figure 4. Seasonal cycles of observed and modeled weekly daytime average fluxes at Kane Forest, PA, from April 29 through October 24, 1997. (a) CO_2 flux (ppm m s^{-1}), (b) H_2O flux (W m^{-2}), (c) O_3 flux (ppb m s^{-1}), and (d) SO_2 flux (ppb m s^{-1}).

ification of V_m in the model would probably give better results for long-term estimation.

3.1.3. Comparisons With the MLM and RADM Models

[27] The MLM and RADM models predict deposition velocities of O_3 and SO_2 , but not CO_2 and H_2O fluxes. Therefore, comparisons between the MLBC and the MLM and RADM models were restricted to the first two chemical species. The values of the correlation coefficient (R), standard deviations (σ_m and σ_o) and the centered pattern root-mean-square difference (E') for the three models at Kane Forest and Nashville were computed and plotted on Taylor's [2001] diagrams.

3.1.3.1. Kane Forest Site

[28] The values of σ_m , σ_o , E' , and R for deposition velocities of O_3 and SO_2 for the three models, as well observations at this site are given in Figures 8a and 8b, respectively. For O_3 deposition velocity, The R -values range from 0.64 cm s^{-1} (RADM) to 0.81 cm s^{-1} (MLBC). This indicates that the MLBC model simulations of O_3 deposition velocity were better in-phase with the simulations from the other two models. It can be seen that the MLBC model had the same standard deviations as the observations, and the other two models had smaller standard deviations. This suggests that the MLM and RADM model underestimated the variability in the diurnal and seasonal cycle amplitudes

of O_3 deposition velocity. The MLBC model has the smallest E' value while the RADM model has the largest one, indicating that the MLBC has the closest overall correspondence to the observations. For SO_2 deposition velocity, the MLBC model also had the largest R -value (0.64). The MLBC model and the observations had similar standard deviations, while the other two models had much smaller standard deviations than the observations. This indicates that the MLBC model correctly estimated the amplitude of variability of SO_2 deposition velocity while the other two models underestimated it. All models had similar E' values.

[29] The seasonal and diurnal cycles of deposition velocity for O_3 and SO_2 at Kane Forest, as illustrated by modeled weekly daytime averages and hourly averages, along with the corresponding averaged observations, are shown in Figures 9 and 10. These figures further confirm the discussion above: the seasonal and diurnal cycles modeled by the MLBC model were in better agreement with observed variations in seasonal and diurnal cycles than the other two models. The observations show that both O_3 and SO_2 deposition velocity have clear seasonal changes, increase in spring, reach maxima in summer, decrease in fall, and reach minima in winter. There are two major peaks, one around week 30, the other around week 35. The MLBC was the only model that predicted both peaks. The diurnal variations of O_3 and SO_2 deposition velocity were even

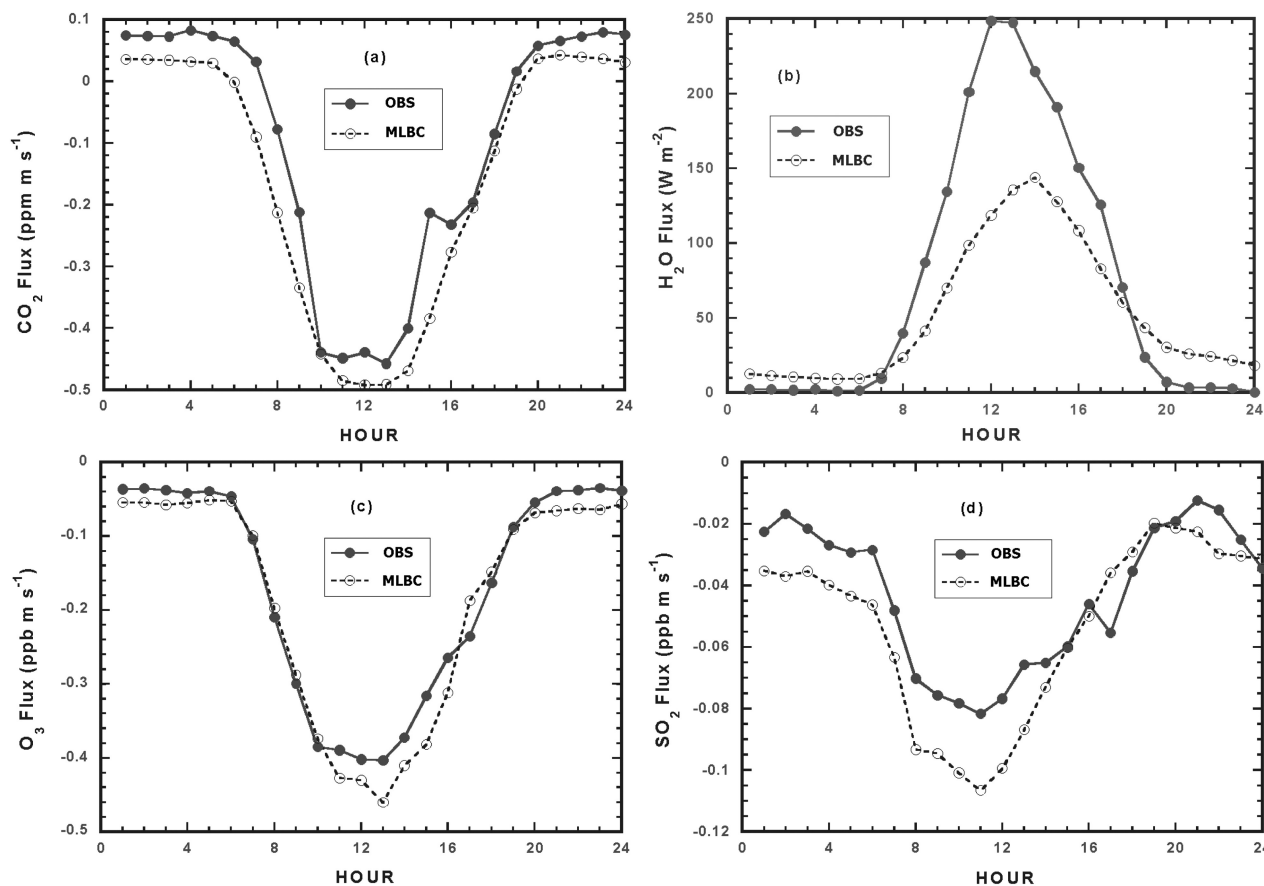


Figure 5. Average diurnal cycles of observed and modeled fluxes at Kane Forest, PA, from April 29 through October 24, 1997. (a) CO_2 flux (ppm m s^{-1}), (b) H_2O flux (W m^{-2}), (c) O_3 flux (ppb m s^{-1}), and (d) SO_2 flux (ppb m s^{-1}).

more significant. The O_3 deposition velocity at night was less than 0.2 cm s^{-1} . It starts to increase around 05:00 and reaches its maximum around 10:00, then begins to decrease. The time of the maximum predicted by MLBC was about one hour later than observed, while the maxima predicted by the other two models were about 3 hours later. The amplitude of the maximum predicted by the MLBC was about the same as observed, while the maxima predicted by the other two models were less than the observed. For SO_2 deposition velocity, both the MLBC and MLM models predicted its diurnal variation, but the RADM completely missed the diurnal variation. The MLBC overestimated the diurnal variation while the MLM underestimated it.

3.1.3.2. Nashville Site

[30] For O_3 deposition velocity (Figure 11), the MLBC model had the largest R -value of 0.84 while the RADM model had the smallest R -value of 0.66. The R -value for the MLM model was 0.71. The standard deviations for the MLBC and MLM model were close to those observed while the RADM model had a much smaller one. The MLBC model also had the smallest E' while the RADM model had the largest one. For SO_2 deposition velocity, the R -values for the MLBC and MLM model were about the same (0.68 and 0.67, respectively), but the RADM model had a much smaller value of 0.50. All modeled standard deviation were smaller than observed, but the MLBC model had the largest

among the three models. Though the MLBC model had the smallest E' value, the E' values for other two models were very close.

[31] As illustrated by the weekly daytime averages and hourly averages of deposition velocity for O_3 and SO_2 in Figures 12 and 13, it is obvious that the seasonal and diurnal cycles of the MLBC model were better correlated with the observations than those of the other two models. There were also two peaks during the seasonal cycle for both O_3 and SO_2 deposition velocity, one around week 32, and the other around week 38. It is believed that the fall-off between the two peaks was due to drought, where the second peak was due to rainfall occurring late in the season. The MLBC successfully predicted these peaks, the MLM predicted the two peaks for O_3 deposition velocity but missed the peaks of SO_2 deposition velocity, and the RADM missed both peaks. The amplitude of the seasonal variation of O_3 deposition velocity predicted by the MLBC is about the same as observed while the other two models underestimated the amplitude. All models underestimated the amplitude of the seasonal cycle of SO_2 deposition velocity. The diurnal variation of O_3 deposition velocity was also significant; the amplitude was about 0.5 cm s^{-1} . The deposition velocity of O_3 at night was about 0.15 cm s^{-1} , increased significantly after 04:00 and reached a peak (0.7 cm s^{-1}) around 08:00, then stepped down to 0.6 cm s^{-1} ,

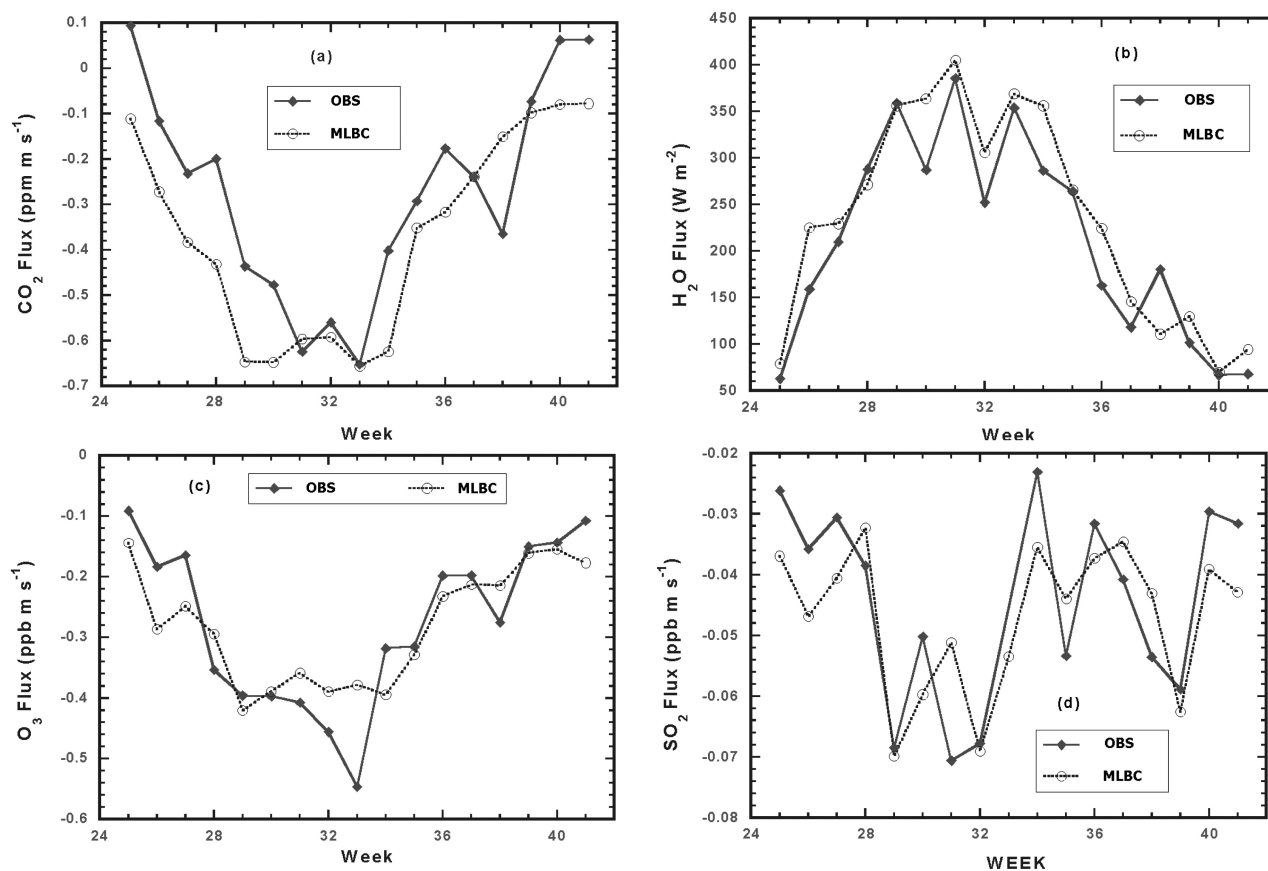


Figure 6. Seasonal cycles of observed and modeled weekly daytime average fluxes at Nashville, TN, from June 22 through October 11, 1995. (a) CO_2 flux (ppm m s^{-1}), (b) H_2O flux (W m^{-2}), (c) O_3 flux (ppb m s^{-1}), and (d) SO_2 flux (ppb m s^{-1}).

and finally rapidly decreased to a minimum before 20:00. The diurnal cycle predicted by the MLBC was in better agreement with the observed cycle than those predicted by the other two models. The MLBC model also predicted the early morning peak of SO_2 deposition velocity while the other models missed it. The diurnal amplitude of SO_2 deposition velocity estimated by the MLBC model was close to the observed while the other two models underestimated it.

3.1.4. Aerodynamic Resistance Formulation

[32] In part 1 of these papers [Wu *et al.*, 2002], the formulation given for the aerodynamic resistance (R_A) term is based on Monin-Obukhov similarity theory with the necessary parameters developed from an estimate of z/L computed from observations of vertical temperature gradient (ΔT) and wind speed. There is some concern [Nakamura and Mahrt, 2001; Hicks, 2001] that similarity theory may not work over complex terrain, and that a simpler, but more robust, technique should be used. Such an approach is used in the MLM [Meyers *et al.*, 1998], in which R_A is estimated from observations of wind speed, the standard deviation of the wind direction (σ_θ), and the time of day.

[33] To address this issue, the MLBC was programmed with a switch to allow R_A to be computed with either of these formulations. Comparisons between the two approaches was done by looking at the agreement between predicted and observed fluxes during the daytime, with the

assumption that an inferior form of R_A would lead to inferior agreement between predictions and observations. The results for H_2O and O_3 at two sites are given in Table 3.

[34] In Table 3, the correlation coefficient (R) and slope of the regression line (M) are given. It is apparent that at each site the differences in model performance caused by differences between models for R_A are small, with the Monin-Obukhov method performing slightly better. The differences are also slightly smaller at the very homogeneous conditions at Plymouth than at the much more varied conditions at Kane. Thus we conclude that the conditions at these sites do not limit the use of Similarity Theory, nor do they make a persuasive argument for the use of the simpler R_A formulation in the MLM.

[35] The sites used for these experiments varied from almost ideal (from a micro-meteorological perspective) to somewhat less than ideal in the forest-covered areas of Pennsylvania and the Adirondack mountains. However, none of these sites suffered from extremely steep terrain, rapid changes in elevation, or discontinuous ground cover, where similarity theory and the very concept of a continuous deposition velocity may have serious errors.

3.2. Model Sensitivities

[36] Sensitivity analyses were performed to investigate the response of the MLBC model to environmental changes and measurement errors. Normalized flux is defined as the

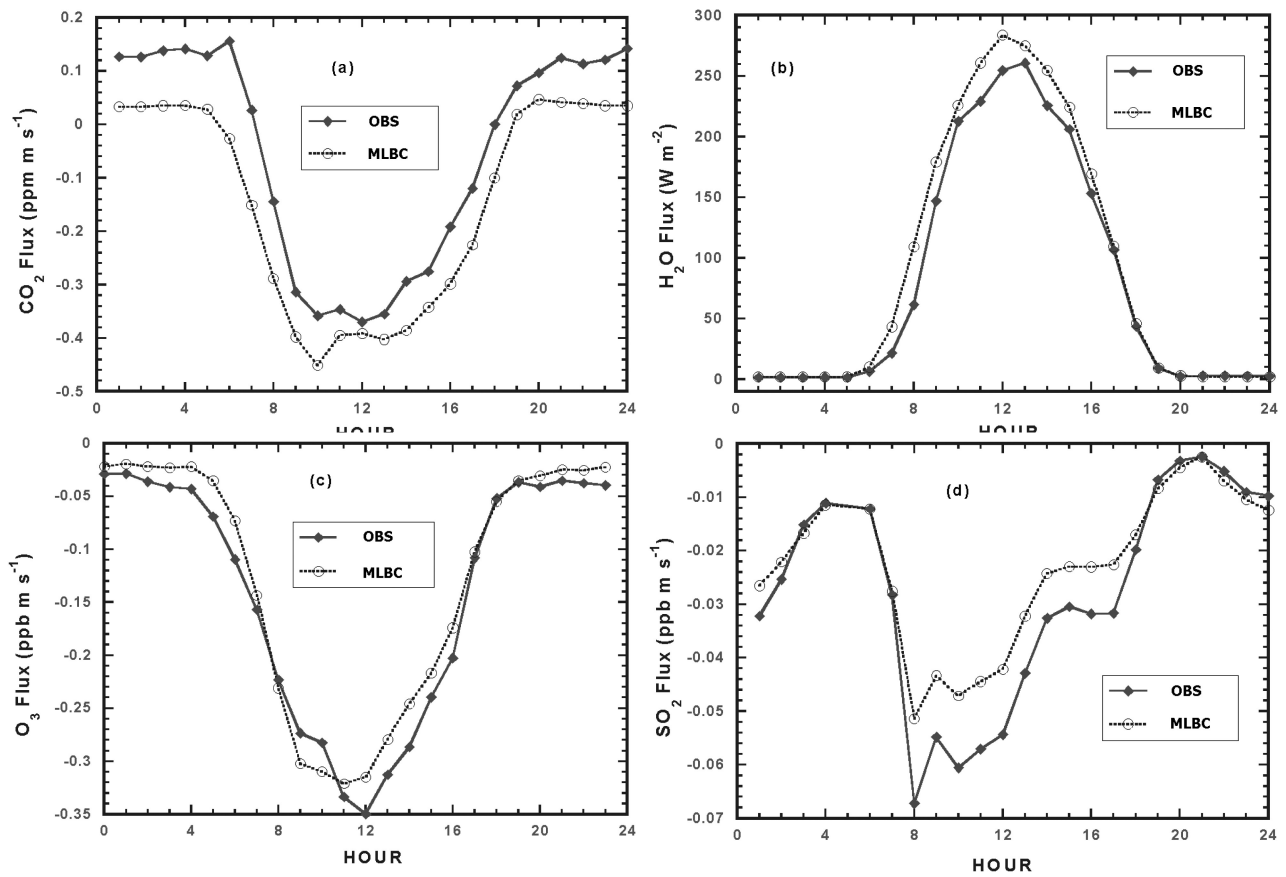


Figure 7. Average diurnal cycles of observed and modeled fluxes at Nashville, TN, from June 22 through October 11, 1995. (a) CO₂ flux (ppm m s⁻¹), (b) H₂O flux (W m⁻²), (c) O₃ flux (ppb m s⁻¹), (d) SO₂ flux (ppb m s⁻¹).

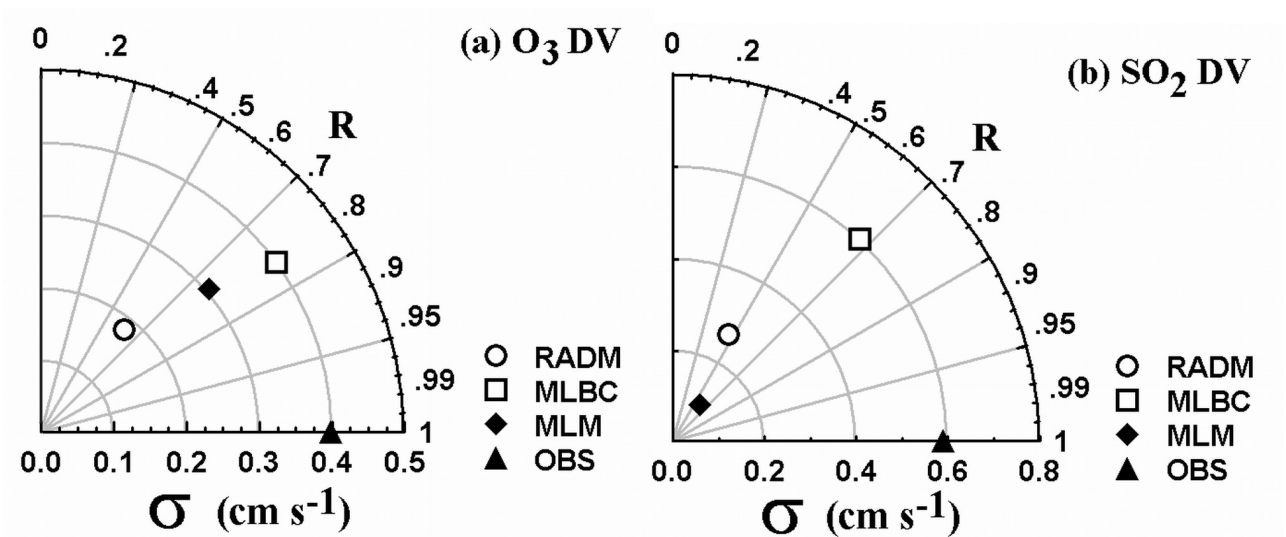


Figure 8. Model comparison for (a) O₃ deposition velocity (cm s⁻¹) and (b) SO₂ deposition velocity (cm s⁻¹) at the Kane Forest, PA, from April 29 through October 24, 1997. The correlation coefficient (*R*), the standard deviation (σ) and the centered pattern root-mean-square difference (*E'*) are shown as in Figure 2.

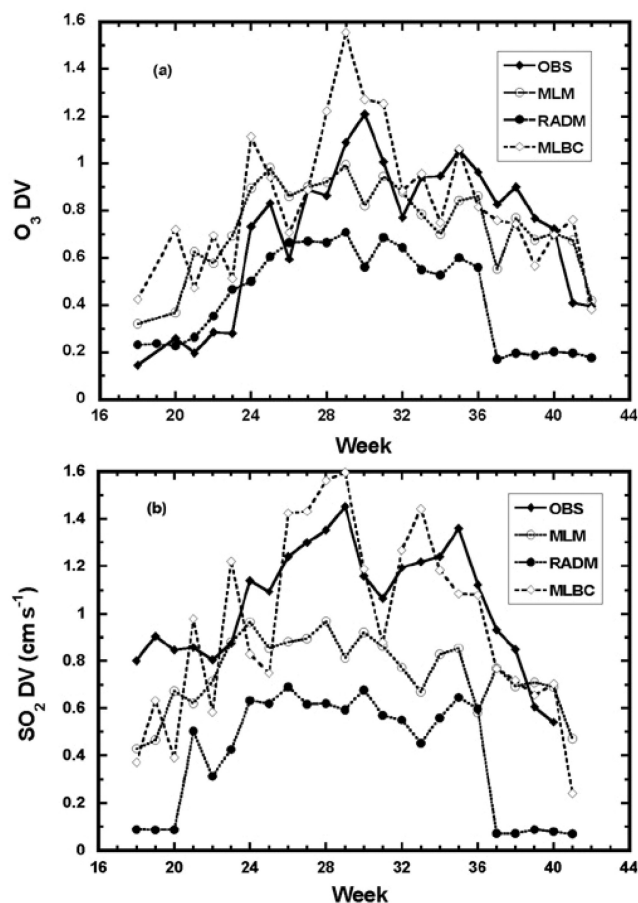


Figure 9. Seasonal cycle of observed and modeled weekly daytime average (a) O_3 deposition velocity (cm s^{-1}) and (b) SO_2 deposition velocity (cm s^{-1}) at Kane Forest, PA, from April 29 through October 24, 1997.

flux divided by the corresponding maximum. Therefore, normalized fluxes vary from zero to unity except CO_2 flux, which is downward most of the time, and upward in the early morning.

3.2.1. Model Response to Environmental Changes

[37] To investigate the model response to environmental changes, typical summer noon conditions at Nashville were chosen as the basic state, and input variables were varied over an expected range of values. Only one input was varied at a time; the rest were held fixed despite the known fact that many inputs are highly correlated. For example, O_3 concentration, relative humidity, air temperature, vertical temperature gradient and solar radiation are all highly correlated and have a strong diurnal cycle. There can be important feedbacks with the change of input variable on the physiological responses, which may be very different in this sensitivity test. Therefore, this procedure for determining the model sensitivities may calculate a deposition velocity for a combination of inputs seldom observed in the real world. This sensitivity test is simple and realistic, and has been used in various model developments. Its results can tell how models behave, and can be checked with the experiments under controlled conditions, such as experiments in chambers. In most cases, it gives variations that are larger than in the real world, but bracket real world

conditions, so that the reader can see both the normal and extreme cases. The basic state values were randomly chosen, taken from hour 12:00 on 1 August 1995 of the Nashville data, and are listed in Table 4.

[38] Figure 14a shows the sensitivity of the modeled CO_2 , O_3 , SO_2 and H_2O (latent heat) fluxes to wind speed, which primarily affects the aerodynamic resistance. As the wind speed increases, the shear-driven turbulence increases, resulting in decreased aerodynamic resistance. Therefore, all of the modeled fluxes increase as wind speed increases, and asymptotically approach their maximum when wind speed is about 10 m s^{-1} . The modeled fluxes are most sensitive to wind speed changes in the range of 0 to 5 m s^{-1} , but not sensitive at all when wind speed is greater than about 12 m s^{-1} . Among the four fluxes, O_3 and SO_2 fluxes are the most sensitive to wind speed changes, and their sensitivities are about the same. H_2O flux is the second-most sensitive one, and CO_2 flux shows the least sensitivity. These suggest that stomatal resistance plays a more important role than aerodynamic resistance in CO_2/H_2O flux exchanges compared with SO_2 and O_3 flux exchanges.

[39] Figure 14b shows the sensitivity of the modeled fluxes of CO_2 , O_3 , SO_2 and H_2O to the vertical temperature gradient (ΔT), which like wind speed affects the aerodynamic resistance. Negative ΔT indicates unstable atmos-

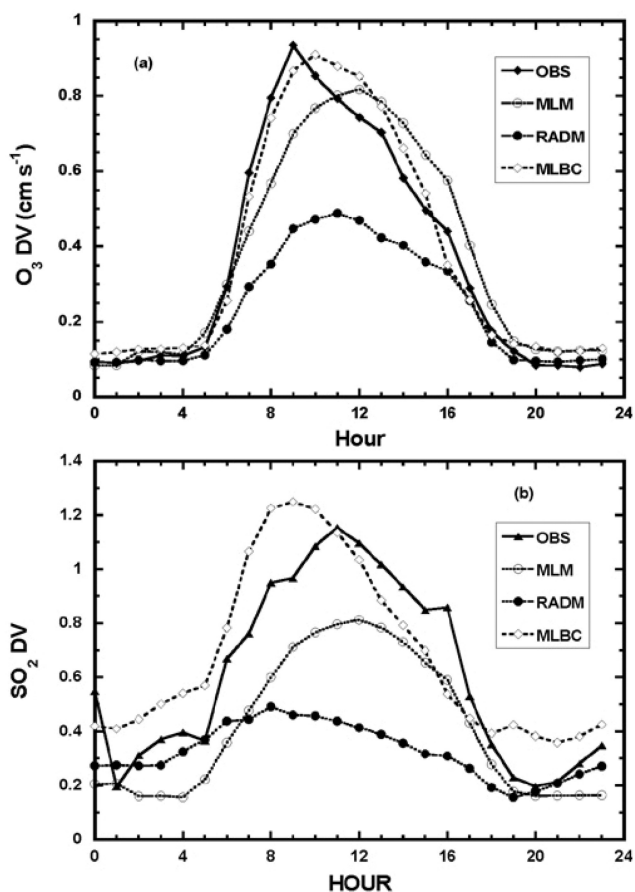


Figure 10. Average diurnal cycle of observed and modeled (a) O_3 deposition velocity (cm s^{-1}) and (b) SO_2 deposition velocity (cm s^{-1}) at Kane Forest, PA, from April 29 through October 24, 1997.

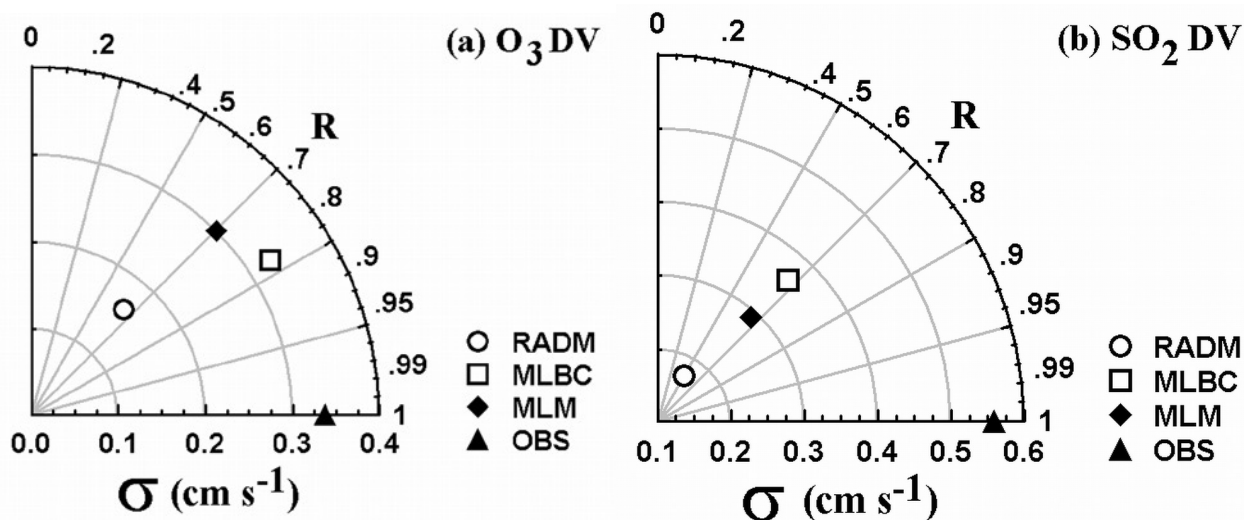


Figure 11. Model comparison for (a) O₃ deposition velocity (cm s⁻¹) and (b) SO₂ deposition velocity (cm s⁻¹) at Nashville, TN, from June 22 through October 11, 1995. The correlation coefficient (*R*), the standard deviation (σ) and the centered pattern root-mean-square difference (*E'*) are shown as in Figure 2.

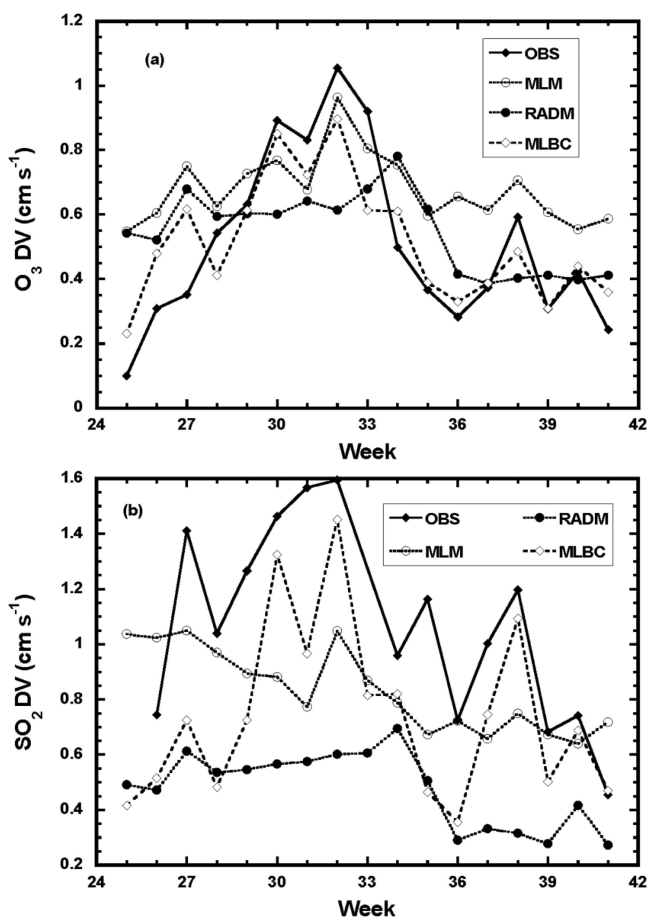


Figure 12. Seasonal cycle of observed and modeled (a) O₃ deposition velocity (cm s⁻¹) and (b) SO₂ deposition velocity (cm s⁻¹) at Nashville, TN, from June 22 through October 11, 1995.

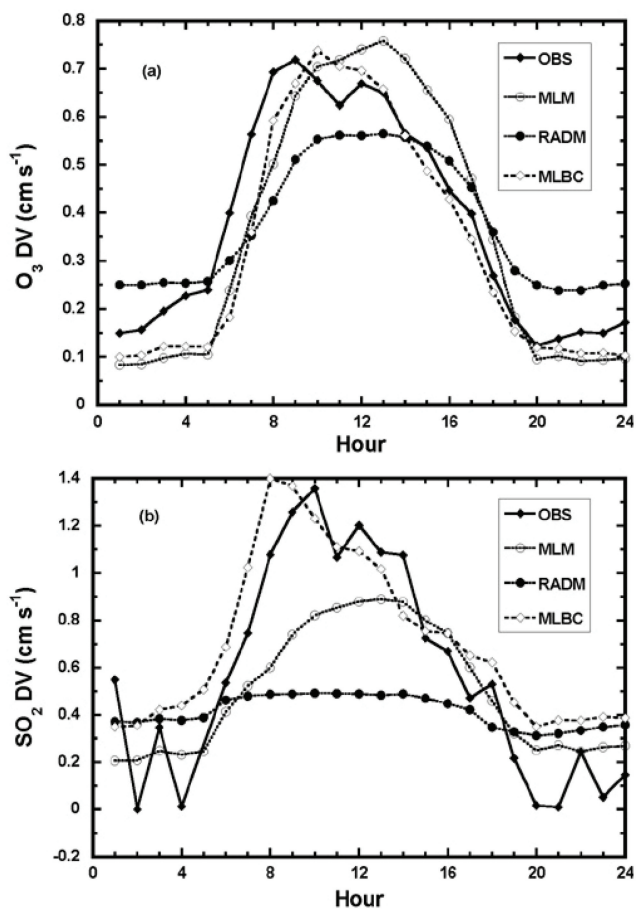


Figure 13. Average diurnal cycle of observed and modeled weekly daytime average (a) O₃ deposition velocity (cm s⁻¹) and (b) SO₂ deposition velocity (cm s⁻¹) at Nashville, TN, from June 22 through October 11, 1995.

Table 3. Comparison of Two Different Aerodynamic Resistance (R_A) Models, by Comparing Modeled Versus Observed Correlation Coefficient, R , and Slope of the Linear Least Squares Fit, M , for Two Sets of Fluxes and Sites

	<i>Meyers et al.</i> [1998]		Monin-Obukhov	
	R	M	R	M
	<i>Plymouth</i>			
H ₂ O	.97	.96	.97	1.01
O ₃	.94	.82	.93	.92
	<i>Kane</i>			
H ₂ O	.88	.81	.91	.81
O ₃	.72	.97	.81	1.15

pheric conditions (high turbulence, low R_A) while positive ΔT represents stable atmospheric conditions (low turbulence, high R_A). All of the modeled fluxes decrease as stratification shifts from unstable to stable. However, the model is more sensitive to the changes of ΔT when the atmosphere is stable as shear-driven turbulence is increasingly suppressed by buoyancy. There are some differences among the four types of fluxes regarding their sensitivity to ΔT : under unstable conditions, CO₂ flux is more sensitive to ΔT changes than the other three fluxes; under stable condition, CO₂ flux is the one with the least sensitivity. Overall, O₃ and SO₂ fluxes are more sensitive to changes in ΔT than H₂O and especially CO₂ fluxes are.

[40] Figure 14c shows the changes of the modeled fluxes with air temperature. Air temperature affect photosynthesis (stomatal resistance), vapor deficit, and diffusivity of gases. However, its dominant effect is on photosynthesis, as shown in the figure. When air temperature is below 30°C, all modeled fluxes increase as air temperature increases. The modeled CO₂ flux reaches its maximum when air temperature reaches 30°C, then decreases as air temperature increases. However, the other three fluxes continue increasing until air temperature reaches about 37°C, then decrease as air temperature increases. Among the four types of fluxes, CO₂ and H₂O fluxes have the most sensitivity while SO₂ flux has the least sensitivity to air temperature changes. This also implies that stomatal resistance plays a more important role in CO₂/H₂O flux exchanges than in SO₂ flux exchanges.

[41] The changes of modeled CO₂, O₃, SO₂ and H₂O fluxes with global solar radiation are shown in Figure 14d. Global radiation primarily affects plant photosynthesis (stomatal resistance). As shown in the figure, all of the modeled fluxes increase as global solar radiation increases until about 800 W m² where plants reach their light saturation point. The CO₂ flux is positive (dominated by plant respiration) when global radiation is below 150 W m², and then becomes negative (dominated by photosynthesis) as global solar radiation increases beyond that value. Therefore, CO₂ Flux is the most sensitive to global radiation changes within this region. Among the four fluxes, CO₂ flux has the most sensitivity while SO₂ flux has the least sensitivity to changes in global solar radiation.

[42] The model is also sensitive to relative humidity. Shown in Figure 14e, stomatal closure is apparent at very low relative humidity. When relative humidity is less than 20%, CO₂ flux is positive (values shown in the figure are normalized by negative CO₂ flux) while the other three

fluxes have their minimum values. As relative humidity increases above 20%, all modeled fluxes increase. CO₂, O₃ and SO₂ fluxes reach their maximum when the air is completely saturated (relative humidity reaches 100%) while latent heat flux reaches its maximum around a relative humidity of 50%. At lower humidity, transpiration is limited by stomatal closure. At higher relative humidity, transpiration is limited by smaller vapor pressure deficit. The modeled CO₂ flux is most sensitive to air humidity in the range around 20 to 40% while the modeled O₃, SO₂ and latent heat flux are sensitive in the whole range from 20 to 100%.

[43] Figure 14f shows the changes of modeled CO₂, O₃, SO₂ and H₂O fluxes with CO₂ concentration. As CO₂ concentration increases, the modeled CO₂ fluxes increases while the modeled O₃, SO₂ and latent heat fluxes decrease. This suggests that an increase in CO₂ concentration causes a reduction in stomatal aperture and an increase in stomatal resistance. This results in a decrease in transpiration. Subsequently, the air near the canopy is dryer, and the vapor deficit between the air and canopy increases, causing further increase in stomatal resistance. As stomatal resistance increases, H₂O, O₃ and SO₂ fluxes decrease. However, CO₂ flux does not because the gradient of CO₂ concentration increases. The increase in modeled CO₂ flux and decrease in modeled transpiration due to increase in CO₂ concentration agree with the experimental result from *Hunsaker et al.* [2000], and the simulation by *Friend and Cox* [1995], *Dugas et al.* [1997], and *Gottschalk et al.* [2001].

3.2.2. Model Response to Measurement Error

[44] To investigate what magnitude of measurement error is acceptable to get reasonable model output, the model was run for two typical cases with an instrument error for each input variables. The first case is a typical morning at Nashville, TN; the inputs values and errors are listed in Table 5. The other case is a typical noontime at Nashville data, and is shown in Table 6. This investigation is intended to find the precision requirements for measured inputs, the error incurred from various assumed parameter values, and to show the range of output values it spans. Errors are taken as typical measurement errors for their respective instruments.

[45] In the early morning of the summer at Nashville, the modeled CO₂ flux is most sensitive to the changes in global solar radiation. An error of 5% in global solar radiation measurement could cause 5% uncertainty in modeled CO₂ flux. In addition, an error of 0.5°C in air temperature can cause a 5% variation in the modeled CO₂ flux while an error of 5% in CO₂ concentration can cause a 3% variation in modeled CO₂ flux. Errors due to the other input parameters are small and could be ignored.

Table 4. Input Variables for the Basic State for Sensitivity Studies^a

Input Variable	Symbol	Value
CO ₂ Concentration	C_a	343.44 ppm
Wind Speed	U_a	2.29 m s ⁻¹
Solar Radiation	R_G	950. W m ⁻²
Atmospheric Pressure	P	999.0 mb
Air Temperature	T_a	34.74°C
Upper-Lower Temperature Difference	ΔT	-0.625°C
Relative Humidity	H	58.11 %
PH Value	PH	4.2731

^aData were randomly chosen from the Nashville site (soybeans) from 12:00 on 1 August 1995.

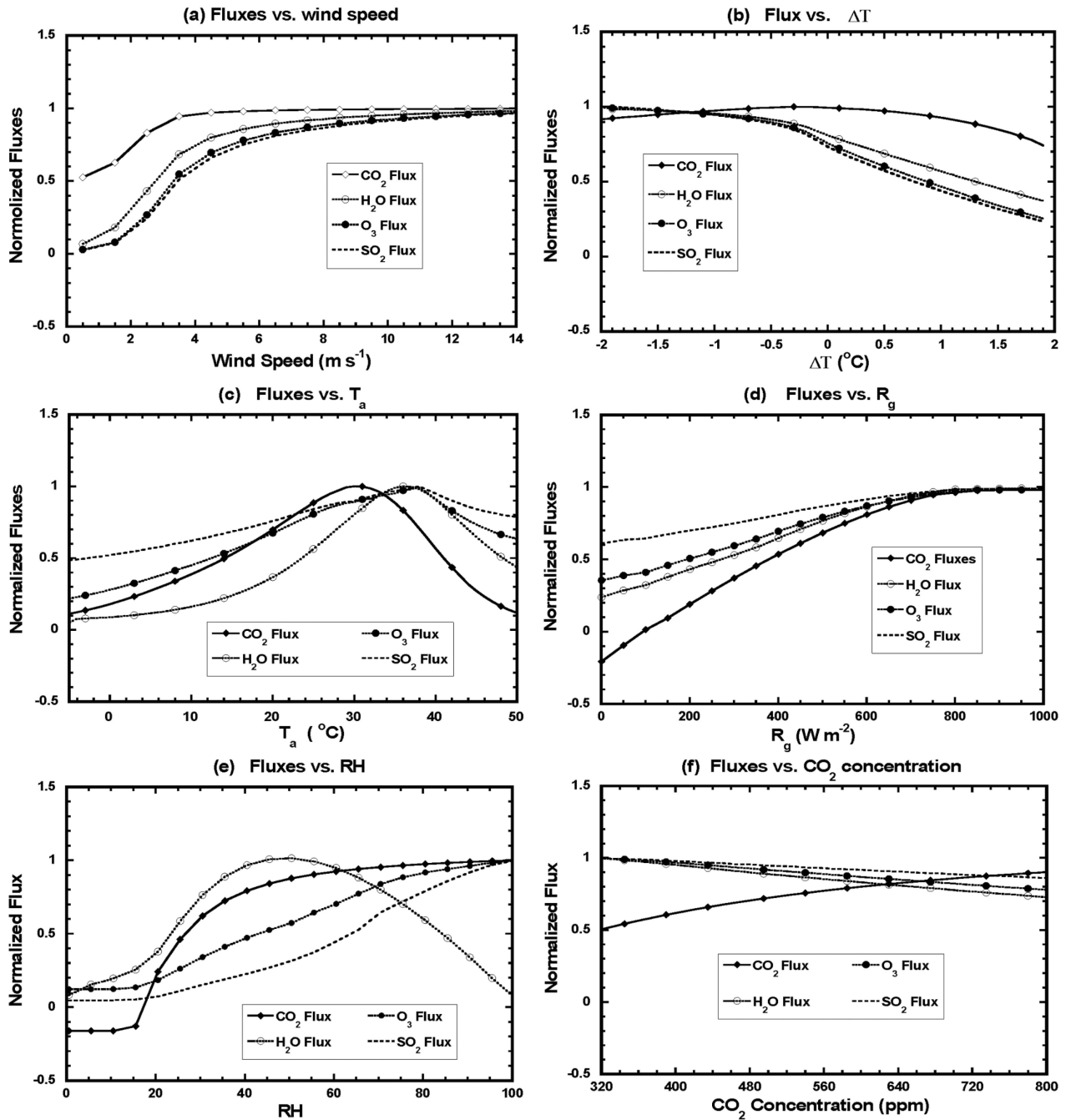


Figure 14. Changes of normalized modeled fluxes with input variables: (a) changes with wind speed, (b) changes with vertical temperature gradient, (c) changes with air temperature, (d) changes with global solar radiation, (e) changes with relative humidity, (f) changes with CO₂ concentration.

Table 5. Relative Changes of CO₂, H₂O, O₃, and SO₂ Fluxes Corresponding to an Increase in Input Variables on a Typical Morning in Summer at Nashville, Tennessee

Input Variables		Changes in Output Fluxes, %			
Variables	Change	CO ₂ flux	H ₂ O Flux	O ₃ Flux	SO ₂ Flux
CO ₂ Concentration (360.0 ppm)	+5%	+2.6	-2.8	-1.9	-0.0
Air Temperature (28.0°C)	+0.5 °C	+0.5	-6.9	-1.8	-0.0
Wind Speed (3.00 m s ⁻¹)	+5%	+0.0	+0.1	+0.2	+2.7
Global Solar Radiation (200 W m ⁻²)	+5%	+5.2	+2.2	+1.1	+0.0
Relative Humidity (75 %)	+5%	+0.7	-16.0	+5.4	+13.5
ΔT (0.0°C)	+0.02°C	-0.0	-0.1	-0.3	-2.7
PH Value (4.2)	+0.5	0.0	0.0	+0.3	+2.8
Pressure (999.0 mb)	0.5 mb	-0.1	-0.1	-0.0	+0.0

Table 6. Relative Changes of CO₂, H₂O, O₃, and SO₂ Fluxes Corresponding to an Increase in Input Variables at a Typical Noontime in Summer at Nashville, Tennessee

Input Variables		Changes in Output Fluxes, %			
Variables	Change	CO ₂ flux	H ₂ O Flux	O ₃ Flux	SO ₂ Flux
CO ₂ Concentration (343.4 ppm)	+5%	+4.9	-0.9	-0.6	-0.3
Air Temperature (34.74°C)	+0.5°C	-3.2	+0.6	-0.8	-0.7
Wind Speed (2.29 m s ⁻¹)	+5%	+0.1	+0.4	+0.7	+0.7
Global Solar Radiation (950.0 W m ⁻²)	+5%	+0.6	+0.5	+0.5	+0.0
Relative Humidity (58.11 %)	+5%	+1.4	-2.0	+5.1	+10.9
ΔT (-0.625°C)	+0.02°C	-0.2	-0.2	-0.3	-0.3
PH Value (4.2731)	+0.5	0.0	0.0	+0.1	+4.4
Pressure (999.0 mb)	0.5 mb	-0.1	-0.2	-0.1	-0.0

[46] The modeled latent heat flux can be affected by the errors in several input variables. The order of the contribution of these input variables to the modeled H₂O flux is relative humidity (16%), air temperature (7%), CO₂ concentration (3%) and global solar radiation (2%). The only input variable, which can cause a variation larger than 3% in the modeled O₃ flux, is relative humidity. For the modeled SO₂ flux, the most important variable is relative humidity, due to the parameterization of the water film coverage on a leaf in the cuticular resistance scheme. The other variables, which can contribute about 3% error in the model SO₂ flux, are PH, vertical temperature gradient, and wind speed.

[47] At midday in summer at Nashville, CO₂ concentration becomes the most important variable for the modeled CO₂ flux. Air temperature is the second most important one. Since air temperature was very high at this time, further increases will result in a reduction in photosynthesis. Global solar radiation is not important in this particular case even though the absolute change is larger than the one in the morning case because conditions were already past the solar radiation saturation point for C₃ plants. It seems that the modeled H₂O flux will not be significantly affected by a variation in any of input variables tested in this case, suggesting that the effect of all input variables on the modeled H₂O flux were at a plateau. In this midday case, a variation of 5% in relative humidity can cause 5% variation in the modeled O₃ flux. The effects of variations in the other input variables on the modeled O₃ flux are not large. Relative humidity is also the most important input variable to the modeled SO₂ flux. An increase of 5% in relative humidity can cause an increase of 14% in the modeled SO₂ flux. Compared to the increase in the morning case, the absolute change is smaller, but the impact is larger.

[48] From the discussion above, it can be concluded that the errors do depend on the accuracy and precision of the measured input variables. A good quality assurance (QA) program is needed to insure the best performance from the model. However, it should be noted that these potential errors due to measurements errors are less than differences between the model predictions and observations.

4. Summary

[49] The multilayer biochemical dry deposition model (MLBC) described by in the accompanying paper was evaluated using half-hourly eddy correlation (EC) data from six field sites under a wide range of climate conditions with various plant types. The model performance was investi-

gated using the single-diagram method described by *Taylor* [2001]. Modeled CO₂, O₃, SO₂ and H₂O fluxes match well with observations at all sites, although some bias is present. Differences of the model outputs between different sites with different plants are not large. The model was also compared with the MLM and RADM models. Comparisons show that the MLBC model is an improvement over the MLM and RADM models. Model sensitivity to the changes of input variables was also conducted. The model produces very reasonable response to the environmental conditions (air temperature, pressure, humidity, wind speed, solar radiation, vertical temperature gradient, CO₂ concentration, etc.), indicating that the model has potential applications to a wide range of climate conditions, and can be used in the Clean Air Status And Trends Network (CASTNet). Analysis shows that stomata are the dominant controlling factor for CO₂, H₂O and O₃ fluxes while cuticular and aerodynamic resistances play important roles for SO₂ flux when the canopy is wet. Statistical analyses suggest that the photosynthesis model works better for C₃ plants than for C₄ plants. The scheme for C₄ plant photosynthesis proposed by *von Caemmerer and Furbank* [1999] considers more variables, and may be worth testing in the future studies. The maximum photosynthetic capacity (V_m) in the model should be specified dynamically for long-term estimates. The model also shows high sensitivity to the changes in relative humidity, indicating that correctly computing water thickness on a leaf surface is very important. Evaporation from wet leaves occurs in real situations but is not considered in the model, resulting in underestimation in both the weekly daytime averages and hourly averages at the Kane Forest site. These suggest that the method developed by *Xiao et al.* [2000] or similar method is worth testing in the future studies. Model outputs depend on the accuracy and precision of input variables and a good QA measurement program is required for good model performance, but most of the sensitivities to typical measurement errors were acceptable, and smaller than the overall error of the model when compared with observations.

[50] **Acknowledgments.** B. Brashers was supported by a National Research Council Postdoctoral fellowship. Yihua Wu is a scientific visitor at the EPA. This position is administered by UCAR Visiting Scientist Programs. This manuscript has been reviewed by NOAAEPA and approved for publication.

References

Dugas, W. A., S. A. Prior, and H. H. Rogers, Transpiration from sorghum and soybean growing under ambient and elevated CO₂ concentrations, *Agric. For. Meteorol.*, 83, 37–48, 1997.

- Finkelstein, P. L., T. G. Ellestad, J. F. Clarke, T. P. Meyers, D. B. Schwede, E. O. Hebert, and J. A. Neal, Ozone and sulfur dioxide dry deposition to forests: Observations and model evaluation, *J. Geophys. Res.*, *105*, 15,365–15,377, 2000.
- Friend, A. D., and P. M. Cox, Modeling the effects of atmospheric CO₂ on vegetation-atmospheric interactions, *Agric. For. Meteorol.*, *73*, 285–295, 1995.
- Gottschalck, J. C., R. R. Gillies, and T. N. Carlson, The simulation of canopy transpiration under doubled CO₂: The evidence and impact of feedback on transpiration in two 1-D soil-vegetation-atmosphere-transfer models, *Agric. For. Meteorol.*, *106*, 1–21, 2001.
- Hicks, B. B., Areal measurements of ozone, water, and heat fluxes over land with different surface complexity, using aircraft, *Water Air Soil Pollut. Focus*, *1*, 213–222, 2001.
- Hunsaker, D. J., B. A. Kimball, P. J. Pinter Jr., G. W. Wall, R. L. LaMorte, F. J. Adamsen, S. W. Leavitt, T. J. Thompson, A. D. Matthias, and T. J. Brooks, CO₂ enrichment and soil nitrogen effects on wheat evaporation and water use efficiency, *Agric. For. Meteorol.*, *104*, 85–105, 2000.
- Meyers, T. P., P. L. Finkelstein, J. Clarke, T. G. Ellestad, and P. Sims, A multilayer model for inferring dry deposition using standard meteorological measurements, *J. Geophys. Res.*, *103*, 22,645–22,661, 1998.
- Nakamura, R., and L. Mahrt, Similarity theory for local and spatially averaged momentum fluxes, *Agric. For. Meteorol.*, *108*, 265–279, 2001.
- Sellers, P. J., S. O. Los, C. J. Tucker, C. O. Justice, D. A. Dazlich, G. J. Collatz, and D. A. Randall, A revised land surface parameterization (SiB2) for atmospheric GCMs, part II, The generation of global fields of terrestrial biophysical parameters from satellite data, *J. Clim.*, *9*, 706–737, 2001.
- Taylor, K. E., Summarizing multiple aspects of model performance in a single diagram, *J. Geophys. Res.*, *106*, 7183–7192, 2001.
- von Caemmerer, S., and R. T. Furbank, Modeling C₄ photosynthesis, in *C₄ Plant Biology*, edited by R. F. Sage and R. K. Monson, chap. 6, pp. 173–211, Academic, San Diego, Calif., 1999.
- Xiao, Q. F., E. G. McPherson, S. L. Ustin, and M. E. Grismer, A new approach to modeling tree rainfall interception, *J. Geophys. Res.*, *105*(D23), 29,173–29,188, 2000.
- Wang, Y. P., and R. Leuning, A two-leaf model for canopy conductance, photosynthesis and partitioning of available energy, I, Model description and comparison with a multi-layered model, *Agric. For. Meteorol.*, *91*, 265–279, 1998.
- Wesely, M. L., Parameterization of surface resistance to gaseous dry deposition in regional-scale numerical models, *Atmos. Environ.*, *23*, 1293–1304, 1989.
- Wilson, K. B., D. D. Baldocchi, and P. J. Hanson, Spatial and seasonal variability of photosynthetic parameters and their relationship to leaf nitrogen in a deciduous forest, *Tree Physiol.*, *20*, 565–578, 2000a.
- Wilson, K. B., D. D. Baldocchi, and P. J. Hanson, Quantifying stomatal and non-stomatal limitations to carbon assimilation resulting from leaf aging and drought in mature deciduous tree species, *Tree Physiol.*, *20*, 787–797, 2000b.
- Wu, Y., B. Brashers, P. Finkelstein, and J. Pleim, A multilayer biochemical dry deposition model, 1 Model formulation, *J. Geophys.*, *107*, doi:10.1029/2002JD002293, in press, 2002.
-
- B. Brashers, MFG Inc, 19203 36th Avenue W, Suite 101, Lynnwood, WA 98036-5707, USA.
- P. L. Finkelstein and J. E. Pleim, Atmospheric Modeling Division, EPA, MD-E243-01, Research Triangle Park, NC 27711, USA.
- Y. Wu, Hydrological Sciences Branch, NASA Goddard Space Flight Center, NASA-GSFC Code 974, Greenbelt, MD 20771, USA. (yw@hsb.gsfc.nasa.gov)